# Cycle-Averaged Models of Cardiovascular Dynamics

Tushar A. Parlikar, *Student Member, IEEE*, Thomas Heldt, *Member, IEEE*, and George C. Verghese, *Fellow, IEEE*

***Abstract*—Lumped-parameter time-varying electrical circuit analogs for the cardiovascular system are frequently used in medical research and teaching for simulating and analyzing hemodynamic data. *Pulsatile* models provide details of the *intra*cycle dynamics of each heart beat. In some settings, however, such as when tracking a hospital patient's hemodynamic state over time, it is more useful to dynamically track the beat-to-beat or *inter*cycle dynamics. Rather than introducing heuristic averaging during the model-building step, as is done in existing nonpulsatile models, we apply a short-term, cycle-averaging operation to the differential equations of the underlying pulsatile model to obtain *cycle-averaged* models. The cycle-averaging method preserves the dependence of the output variables on the model parameters. In this paper, we apply cycle averaging to a simple pulsatile cardiovascular model to derive a cycle-averaged model for cardiovascular dynamics. The resultant model captures the intercycle dynamics with relatively small approximation errors for a large range of perturbations in important system parameters.**

***Index Terms*—Cardiovascular dynamics, cycle-averaged models, cycle averaging, nonpulsatile models, patient monitoring, pulsatile models.**

## I. Introduction

### A. Background

Medical teaching and research have a rich tradition of using simple mechanical or electrical models to describe and elucidate cardiovascular phenomena. This tradition dates back over a century to the work of Frank and his associates, who used a lumped-parameter mechanical model of the arterial system to analyze the arterial pressure pulse [2], [3] and from this estimated cardiac stroke volume [4]. Such models were later implemented on analog computers [5], and subsequently in software on digital computing platforms. These models—particularly in the form of electrical circuit analogs—have been used in teaching physiology [6], [7], as well as in the research setting, where they aid in the interpretation of experimental observations, serving as a rational framework that either links an intervention to the observed system-level response (the *forward* problem) or a system-level observation to the underlying changes in the cardiovascular system (the *inverse* problem).

Manuscript received October 4, 2005; revised July 17, 2006. This paper was presented in part at the 2005 Annual Conference of the IEEE Engineering in Medicine and Biology Society, Shanghai, China, September, 2005. This work was supported in part by the National Institute of Biomedical Imaging and Bioengineering under Grant 1 RO1 EB001659, and in part by the National Aeronautics and Space Administration (NASA) under the NASA Cooperative Agreement NCC 9-58 with the National Space Biomedical Research Institute. This paper was recommended by Guest Editor G.-Z. Yang.

The authors are with the Laboratory for Electromagnetic and Electronic Systems, Massachusetts Institute of Technology, Cambridge, MA 02139 USA (e-mail: parlikar@mit.edu).

Digital Object Identifier 10.1109/TCSI.2006.884457

Integration and interpretation of hemodynamic data streams are particularly important in the clinical environment of the intensive care unit (ICU), where patients are typically heavily instrumented and frequently physiologically unstable. Given the vast amount of clinical information collected from each patient in intensive care, computational models can play an important role in integrating a patient's hemodynamic data streams into a common framework, analyzing and interpreting the available information, and presenting resultant pathophysiological hypotheses to the clinical staff in an efficient manner [8]. To employ computational models in such a way, one needs to match the model structure to the characteristics of the data streams collected at the patient's bedside. This matching must be done both in terms of the time scales involved and the computational complexity of the forward and inverse problems to be solved. In developing cycle-averaged models of cardiovascular dynamics from pulsatile ones, we aim to expand the repertoire of model structures available for matching to clinical data.

### B. Pulsatile, Nonpulsatile, and Cycle-Averaged Models

Models of cardiovascular dynamics are called *pulsatile* if they capture the intrabeat (or intracycle) features of individual pressure, flow, and volume waveforms. Pulsatile behavior can be simulated by lumped-parameter circuit models in which the cardiac chambers are modeled as time-varying capacitors that cycle between a low (systolic or ejection) state and a high (diastolic or filling) state. To understand and/or simulate interbeat (or intercycle) dynamics, however, these models tend to be too detailed and computationally burdensome, as the simulation time step generally has to be chosen much shorter than the cardiac cycle length.

*Nonpulsatile* models simulate the time-average behavior of cardiovascular variables and thus reduce the computational overhead associated with pulsatile models [9], [10]. In order to derive nonpulsatile models, an implicit averaging step has to be taken to transform the pulsatile nature of cardiac outflow to an average flow over the cardiac cycle. For example, Kappel and Peer [10], based on work by Grodins [9], used a heuristic formula to relate stroke volume to average ventricular end-diastolic volume, which in turn they related to average pre- and after-load and average cardiac contractility. Similarly, Boyers and co-workers [11] made stroke volume a function of average central blood volume and average autonomic activity.

Rather than introducing heuristic averaging during the model-building step, one can apply a short-term cycle-averaging operation to the differential equations of the underlying pulsatile model. Such an approach, with certain systematic approximations, leads to *cycle-averaged* models, and has found much applicability in the area of power electronics [12]. The cycle-averaging process preserves the dependence of the output variables on the model parameters, which is a fundamental

advantage over the *a priori* determination of such relationships during the model-building step for nonpulsatile models. In some cases, linear and time-invariant cycle-averaged models can be derived for nonlinear, time-varying pulsatile models [13]. A rich set of analysis tools can then be applied to these cycle-averaged models.

### C. Goals and Outline of the Paper

In this paper, we show how to derive a cycle-averaged model from a pulsatile model. Such cycle-averaged models are intended for use in tracking patient hemodynamic state and parameters in the ICU.

There are several simplifying assumptions we have made in our models of cardiovascular dynamics. We assume the elements in the systemic (or peripheral) circulation are linear and time invariant (LTI). Although LTI inertial and distributed-parameter effects are easily incorporated into the averaging framework, we omit them as they are relatively insignificant for the slow intercycle variations we intend to capture with our cycle-averaged models. Similarly, we neglect the baroreflex and cardiopulmonary control mechanisms that, on a beat-to-beat timescale, tightly control mean arterial blood pressure (ABP). These mechanisms act on time scales of a heart cycle or longer, however, they typically use cycle-averaged rather than instantaneous (or pulsatile) quantities as their inputs [14], [15]. Thus, it is not necessary to model them for purposes of deriving a cycle-averaged model. Instead, once a cycle-averaged model has been obtained, the various control loops can be wrapped around it if required.

The outline of this paper is as follows. In Section II, we describe the basic cycle-averaging methodology and apply it to the well-known Windkessel model [2], [3]. In Section III, we describe the pulsatile cardiovascular model to which we later apply the cycle-averaging methodology. After some additional background on cycle averaging in Section IV, we derive in Section V a cycle-averaged representation for the pulsatile cardiovascular model introduced in Section III. Simulation results obtained using this cycle-averaged model are presented and evaluated in Section VI. We end with a summary and directions for future work.

## II. Cycle-Averaged Windkessel Model

The Windkessel model, whose circuit representation appears in Fig. 1, was originally used to model the ABP pulse [2], [3]. The electric circuit analogs for cardiovascular variables and components (not all present in Fig. 1) are: current $I$ for blood flow, voltage $V$ for blood pressure, charge $Q$ for blood volume, ideal diodes $D$ for heart valves, resistance $R$ for valvular or vascular resistance to blood flow, inductance $L$ for blood inertia, and capacitance $C$ for vascular or compartmental compliance. Elastance $E$ is defined as the inverse of capacitance or compliance. In the Windkessel circuit, $R_a$ is the total peripheral resistance, while $C_a$ is the lumped compliance of the arterial tree. The pressure drop across $R_a$ is the ABP $V_a(t)$. The heart's output $I(t)$ is modeled as an impulsive current source given by

$$I(t) = \mathrm{SV} \sum_n \delta(t - t_n) \tag{1}$$

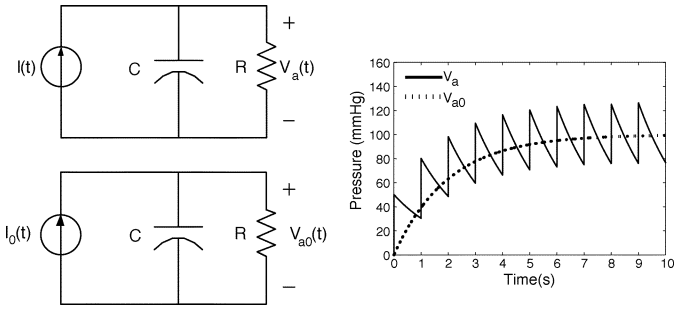


Fig. 1. Windkessel (top) and cycle-averaged Windkessel (bottom) model circuit representations with representative pulsatile and cycle-averaged ABP waveforms.

where SV is the stroke volume and $t_n$ is the onset time of the $n$th cardiac cycle.

The state-space equation for the Windkessel circuit is as follows:

$$\frac{dV_a}{dt} + \frac{V_a}{R_a C_a} = \frac{I}{C_a} \tag{2}$$

where the time argument $t$ has been dropped for simplicity.

The pulsatile ABP waveform that results from simulating the model (2) with $V_a(0) = 0$ is shown in Fig. 1. The pulse pressure (maximum ABP–minimum ABP), $V_{\mathrm{pulse}}$, in each cardiac cycle is given by

$$V_{\mathrm{pulse}} = \frac{\mathrm{SV}}{C_a}. \tag{3}$$

We now describe the basic cycle-averaged methodology (see [12], [16], [17]) and apply it to the Windkessel model to derive the cycle-averaged Windkessel model. Our starting point is the complex Fourier series representation for a signal $x(\tau)$ on the interval $[t - T, t]$, which can be written as

$$x(\tau) = \sum_{k=-\infty}^{\infty} X_k(t) e^{jk\frac{2\pi}{T}\tau}. \tag{4}$$

The $X_k(t)$ are the complex Fourier series coefficients, also referred to as the Index-$k$ cycle averages of $x(\tau)$ and thus denoted by $\langle x \rangle_k(t)$. These complex coefficients are given by

$$X_k(t) = \langle x \rangle_k(t) = \frac{1}{T} \int_{t-T}^{t} x(\tau) e^{-jk\frac{2\pi}{T}\tau} d\tau \tag{5}$$

thanks to the orthogonality properties of the basis functions $\{e^{-jk(2\pi/T)\tau}\}$ on an interval of length $T$. For any real signal $x(t)$, $X_k$ and $X_{-k}$ are complex conjugates

$$X_k = X_k^R + jX_k^I = X_{-k}^* \tag{6}$$

where the superscripts $R$ and $I$ denote real and imaginary parts, and $^*$ denotes complex conjugation.

If $x(\tau)$ were strictly periodic with period $T$, then the $X_k(t)$ would be constants, independent of $t$. For waveforms that deviate only slowly and/or slightly from such periodicity, which is the case of interest to us, it is reasonable to assume that the $X_k(t)$ will have only slow and/or slight departures from constant values, and this can be exploited when making modeling approximations.

From (5), with $k = 0$, we obtain the standard formula for the cycle average of the variable $x(t)$, namely

$$X_0(t) = \langle x \rangle_0(t) = \frac{1}{T} \int_{t-T}^{t} x(\tau) d\tau. \tag{7}$$

This Index-0 cycle average is simply the dc term in the Fourier series (4), and is also the short-term average of the variable $x(t)$ that we wish to track in our cycle-averaged models. We will often simply write $\langle x \rangle(t)$ for $\langle x \rangle_0(t)$. In the cardiovascular circuit models where we apply these expressions, $T$ is the length of the cardiac cycle, assumed to be known and essentially constant over the analysis interval of interest, though possibly different from one analysis interval to another.

By differentiating (5) under the assumption of constant $T$ and setting $k = 0$, we obtain an expression for the derivative of the Index-0 cycle average

$$\frac{d}{dt} X_0(t) = \frac{d}{dt} \langle x \rangle_0(t) = \left\langle \frac{dx}{d\tau} \right\rangle_0 (t). \tag{8}$$

By applying (7) and (8) to the state-space equation (2) for the Windkessel circuit, and taking note of (1), we obtain the following Index-0 cycle-averaged Windkessel model (one could also directly average the circuit, see [18]):

$$\frac{dV_{a0}}{dt} + \frac{V_{a0}}{R_a C_a} = \frac{I_0}{C_a} = \frac{\mathrm{SV}}{C_a T}. \tag{9}$$

It follows from (9) that in steady state we have the following relation between SV and $V_{a0}$:

$$\mathrm{SV} = \frac{V_{a0} T}{R_a}. \tag{10}$$

It follows from (3) and (10) that $V_{\mathrm{pulse}}$ is given by

$$V_{\mathrm{pulse}} = \frac{V_{a0} T}{C_a R_a}. \tag{11}$$

Because the pulsatile Windkessel model is LTI, the cycle-averaged Windkessel model (9) has the same governing differential equation and circuit representation as the pulsatile Windkessel model (2). Of interest is the fact that the time constant in both the pulsatile and the cycle-averaged Windkessel models is $R_a C_a$.

Fig. 1 shows the pulsatile ABP waveform from a simulation of the Windkessel model (an analytical solution is also straightforward), along with the cycle-averaged ABP waveform obtained from a simulation of a cycle-averaged Windkessel model. The time constant with which the average rises to its steady state equals the time constant of the decay on each pulse. It is clear that in order to capture the transient beat-to-beat ABP dynamics, it would for many purposes suffice to capture its cycle average, and that the averaged model is well-suited to efficiently representing the dynamics of the cycle average.

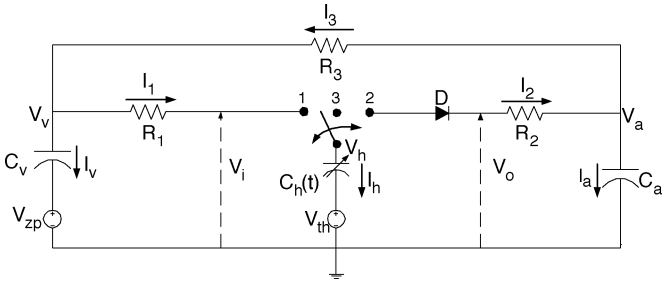


Fig. 2. SPCVM uses a 3-way switch which allows for simpler analysis of the circuit. $V_i$ and $V_o$ are defined here for future reference. For simplicity, only one diode is used, unlike in the models in [13] and [19], to facilitate development of the averaged model.

## III. Simple Pulsatile Cardiovascular Model

When a circuit has nonlinear and/or time-varying elements, cycle averaging is not as easily applied as in the Windkessel case. In this section, we turn to a more elaborate but more realistic model that is time varying and nonlinear; we apply cycle averaging to this model in the next section. This model, the simple pulsatile cardiovascular model (SPCVM), was studied in [13], [19] (see also [20]). It has a single ventricular compartment, and is useful in studying systemic vascular conditions such as hemorrhaging in the peripheral circulation. Fig. 2 illustrates the circuit representation for the SPCVM, where $C_a$ is the arterial compliance, $C_v$ is the venous compliance, $C_h(t)$ is the time-varying ventricular compliance, $R_1$ is the inflow resistance to the ventricle, $R_2$ is the outflow resistance from the ventricle, and $R_3$ is the total peripheral resistance. The voltage $V_h$ is the ventricular pressure, $V_v$ is the central venous pressure (CVP),[1] and $V_a$ is the ABP. The ventricular volume is $Q_h$. The voltage source $V_{\mathrm{zp}}$ is the zero-pressure filling volume for the body's veins, while $V_{\mathrm{th}}$ is the pressure in the thoracic cavity.

The elastance function $E_h(t) = 1/C_h(t)$ for the ventricular compartment in the SPCVM is taken to be a piecewise-linear periodic function

$$E_h(t) = \begin{cases} \frac{(E_s - E_d)}{\frac{T}{3}} t + E_d, & \text{for } 0 \le t \le \frac{T}{3} \\ \frac{(E_s - E_d)}{\frac{T}{6}} \left( \frac{T}{3} - t \right) + E_s, & \text{for } \frac{T}{3} \le t \le \frac{T}{2} \\ E_d, & \text{for } \frac{T}{2} \le t \le T \end{cases} \tag{12}$$

where the period $T$ is the duration of the cardiac cycle, $E_s$ is the end-systolic elastance, and $E_d (\ll E_s)$ is the end-diastolic elastance. Such a time-varying elastance function approximates human data quite well [21].

The parameters used in the SPCVM, including the initial conditions for our simulations, are given in [1]. These parameters represent typical values for a 70-kg male human [22], and, when used with (12), result in reasonable approximations of the waveforms during the cardiac cycle. For simplicity, throughout this paper we have set $V_{\mathrm{zp}}$ and $V_{\mathrm{th}}$ equal to 0 mm Hg. The derivation of a cycle-averaged model with nonzero $V_{\mathrm{zp}}$ and/or $V_{\mathrm{th}}$ would require only a trivial modification of the cycle-averaged model derived here.

[1]The pressure across $C_v$ is more analogous to peripheral venous pressure, but we nevertheless refer to it as CVP here.

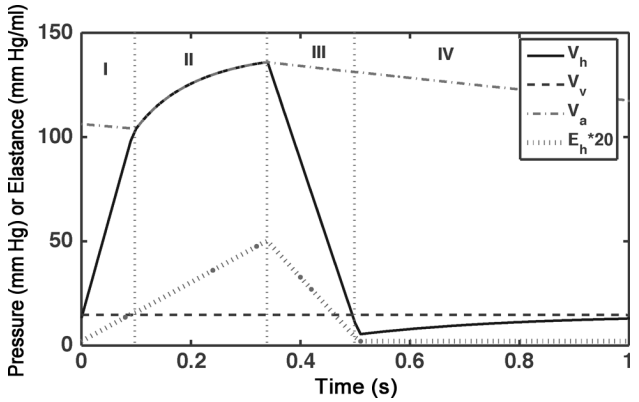


Fig. 3. Waveforms generated over a single cardiac cycle of the SPCVM with $T = 1$ s. This circuit has four regions of operation.

TABLE I
DEFINITION OF THE FOUR REGIONS IN THE SPCVM

| Region | Switch State | Diode State |
|---|---|---|
| I (isovolumic contraction) | $s_2$=1 | $s_D$=0 |
| II (ejection) | $s_2$=1 | $s_D$=1 |
| III (isovolumic relaxation) | $s_3$=1 | $s_D$=0 |
| IV (filling) | $s_1$=1 | $s_D$=0 |

We can define switching functions for the switch and diode in the SPCVM as follows: $s_1(t)$ equals 1 when the switch is in position 1, and 0 otherwise; $s_2(t)$ equals 1 when the switch is in position 2, and 0 otherwise; $s_3(t)$ equals 1 when the switch is in position 3, and 0 otherwise; and $s_D(t)$ equals 1 when the diode $D$ is conducting (between $t = t_D$ and $t = T/3$), and 0 otherwise.

The SPCVM has four regions of operation, corresponding directly with the four periods of the cardiac cycle: isovolumic contraction (I), ejection (II), isovolumic relaxation (III), and filling (IV), as shown in Fig. 3. The four regions are determined by the position of the switch and the state of the diode, as shown in Table I.

With the switching functions described above, and with $Q_h(t)$, $V_a(t)$ and $V_v(t)$ as state variables,[2] we have a state-space description for the SPCVM given by

$$\frac{dQ_h}{dt} = \frac{s_1(V_v - E_h Q_h)}{R_1} + \frac{s_D(V_a - E_h Q_h)}{R_2} \tag{13}$$

$$C_a \frac{dV_a}{dt} = \frac{s_D(E_h Q_h - V_a)}{R_2} + \frac{(V_v - V_a)}{R_3} \tag{14}$$

$$C_v \frac{dV_v}{dt} = \frac{s_1(E_h Q_h - V_v)}{R_1} + \frac{(V_a - V_v)}{R_3} \tag{15}$$

where the parameters $p = \{R_1, R_2, R_3, C_a, C_v, E_s, E_d, T\}$ are fixed or slowly varying, and we have again dropped the time argument $t$ for notational simplicity. More compactly, we can write

$$\frac{d}{dt}\mathbf{x} = \mathcal{A}(s_1, s_D, p)\mathbf{x} \tag{16}$$

[2] $Q_h(t)$ is used as a state variable instead of $V_h(t)$ because it ensures smaller numerical errors, as the term $dC_h(t)/dt$ does not appear in the state-space model.

where $\mathbf{x}$ is the vector of state variables, and the matrix $\mathcal{A}(s_1, s_D, p)$ is equal to

$$\begin{bmatrix} -\frac{(s_1R_2+s_DR_1)E_h}{R_1R_2} & \frac{s_D}{R_2} & \frac{s_1}{R_1} \\ \frac{s_DE_h}{C_aR_2} & -\frac{(s_DR_3+R_2)}{C_aR_2R_3} & \frac{1}{C_aR_3} \\ \frac{s_1E_h}{C_vR_1} & \frac{1}{C_vR_3} & -\frac{(s_1R_3+R_1)}{C_vR_1R_3} \end{bmatrix}. \tag{17}$$

The cycle averaging for this model is considerably more involved than for the Windkessel model, due to the presence of state-dependent switching functions.

## IV. CYCLE-AVERAGE EXPRESSIONS FOR THE SPCVM

To apply the cycle-average operators to our state-space model in (13)–(15), we need additional expressions for derivatives of Index-$k$ cycle averages and for the cycle averages of the products of two variables, such as $s_D(t)V_a(t)$, or three variables, such as $s_1(t)E_h(t)Q_h(t)$.

By differentiating (5) with fixed $T$, we easily obtain an expression for the derivative of the Index-$k$ cycle average

$$\frac{d}{dt}X_k(t) = \left\langle \frac{dx}{d\tau} \right\rangle_k (t) - jk\frac{2\pi}{T}X_k(t). \tag{18}$$

The Index-$k$ cycle average of the product of two signals $x(t)$ and $y(t)$ is given by the easily verified discrete convolution formula for the product of the coefficients of two polynomials

$$\langle xy \rangle_k = \sum_{m=-\infty}^{\infty} X_m Y_{k-m} \tag{19}$$

where we have once more dropped the time argument $t$ from the expression for notational simplicity. The Index-$k$ cycle average of the product of three signals, $x(t)$, $y(t)$, and $z(t)$, can be obtained by applying the discrete convolution relationship (19) to $[x(t)y(t)]z(t)$.

In our application, we can neglect many of the Fourier series coefficients, making these formulas much simpler to apply. Assuming only the Index-0 and Index-1 cycle averages are significant, we have

$$\langle xy \rangle_0 = X_0Y_0 + 2\left(X_1^RY_1^R + X_1^IY_1^I\right) \tag{20}$$

$$\langle xy \rangle_1^R = X_0Y_1^R + X_1^RY_0 \tag{21}$$

$$\langle xy \rangle_1^I = X_0Y_1^I + X_1^IY_0 \tag{22}$$

$$\langle xyz \rangle_0 = X_0\langle yz \rangle_0 + 2\left(X_1^R\langle yz \rangle_1^R + X_1^I\langle yz \rangle_I^I\right) \tag{23}$$

$$\begin{aligned}\langle xyz \rangle_1^R = {} & X_0\langle yz \rangle_1^R + X_1^R\langle yz \rangle_0 + X_1^R\left(X_1^RY_1^R - X_1^IY_1^I\right) \\ & - X_1^I\left(X_1^RY_1^I + X_1^IY_1^R\right)\end{aligned} \tag{24}$$

$$\begin{aligned}\langle xyz \rangle_1^I = {} & X_0\langle yz \rangle_1^I + X_1^I\langle yz \rangle_0 + X_1^I\left(X_1^RY_1^R - X_1^IY_1^I\right) \\ & + X_1^R\left(X_1^RY_1^I + X_1^IY_1^R\right).\end{aligned} \tag{25}$$

To obtain a cycle-averaged model, one can simply apply the formulas derived in Section II and in this section to a state-space model. If we represent circuit variables by their Index-0 and Index-1 (and, when necessary, Index-2) cycle averages, but keep the Index-1 and any Index-2 cycle-averages constant, we end up with what we shall call an *Index-0 cycle-averaged model*.

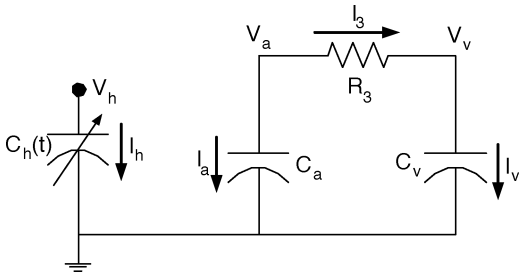


Fig. 4. Circuit schematic for the SPCVM in Region I.

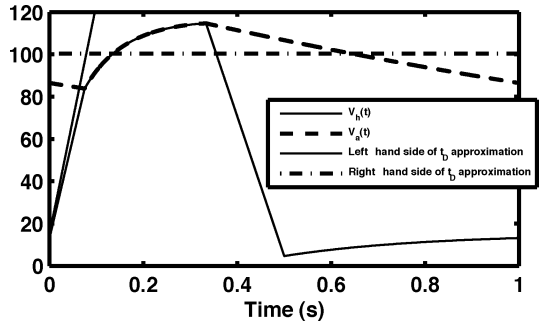


Fig. 5. LHS and RHS of the approximation of the equation defining $\hat{t}_D$. The left-most intersection of $V_h$ and $V_a$ defines $t_D$, while the LHS and RHS of (28) define $\hat{t}_D$.

## V. Index-0 Cycle-Averaged Model

To obtain an Index-0 cycle-averaged model for the SPCVM, we begin by deriving an approximation for the diode turn-on time $t_D$.

### A. Approximation for $t_D$

We first need to express the Index-0 cycle average $S_{D0}$ of the switching function $s_D$ for the diode $D$ in terms of cycle averages of $V_a$, $Q_h$, and $V_v$. We do not require such an approximation for the other switching functions because their Index-0 cycle averages are not state-dependent. An approximation for $t_D$ can be obtained on examination of the relevant circuit waveforms in Region I (see Table I) of the model's operation. In the discussion that follows, we drop the time argument $t$ for notational simplicity.

Fig. 4 shows the SPCVM circuit in Region I, where the switch is in position 2 and the diode $D$ is open. In this region, the charge $Q_h$ is fixed, but pressure $V_h$ is increasing since the elastance function $E_h$ is increasing linearly. At the same time, the arterial pressure $V_a$ is decreasing as $C_a$ discharges into $C_v$. The diode $D$ begins conducting when $V_h$ equals $V_a$.

Since the capacitance $C_v$ is very large, we can assume $V_v$ is essentially constant, and hence that $V_v = V_{v0}$, where $V_{v0}$ is the Index-0 cycle average of $V_v$. Assuming Region I begins at time $t = 0$, $V_h$ in Region I is given by

$$V_h = Q_h E_h = Q_h(0)\left(\frac{(E_s - E_d)}{\frac{T}{3}}t + E_d\right) \tag{26}$$

where we have used the fact that $Q_h = Q_h(0)$ in Region I.

At the beginning of Region I, $V_h \approx V_v$ and $E_h = E_d$, so

$$Q_h(0) \approx \frac{V_{v0}}{E_d}. \tag{27}$$

If we assume the relative ripple on the arterial pressure $V_a$ to be small,[3] we can assume that $V_a = V_{a0}$. The approximate diode turn-on time, $\hat{t}_D$, is then given by solving

$$\begin{aligned} &V_h(\hat{t}_D) = V_a(T + \hat{t}_D) \\ &\frac{V_{v0}}{E_d}\left(\frac{3(E_s - E_d)}{T}\hat{t}_D + E_d\right) = V_{a0} \end{aligned} \tag{28}$$

for $\hat{t}_D$, which yields

$$\hat{t}_D = \frac{E_d T}{3(E_s - E_d)}\left(\frac{V_{a0}}{V_{v0}} - 1\right). \tag{29}$$

Fig. 5 plots both sides of (28) on the same axes as the steady-state waveforms for $V_h$ and $V_a$ obtained with the nominal SPCVM parameters in [1]. The actual $t_D$ is given by the left-most intersection of $V_h$ and $V_a$, while $\hat{t}_D$ is given by the intersection of the lines representing the left-hand side (LHS) and right-hand side (RHS) of (28). The error in approximating $t_D$ is only about 4% for the steady-state waveforms shown in Fig. 5.

The Index-0 cycle average of the $s_D$ waveform is then given by applying the Index-0 cycle-averaging operator to $s_D$ to obtain

$$S_{D0} = \frac{1}{T}\int_{t_D}^{\frac{T}{3}} s_D(t)dt \approx \frac{1}{3} - \frac{E_d}{3(E_s - E_d)}\left(\frac{V_{a0}}{V_{v0}} - 1\right). \tag{30}$$

If we were to approximate $t_D$ as a fixed constant, the resulting Index-0 cycle-averaged model would be linear and time-invariant. However, $S_{D0}$ in (30) depends nonlinearly on state variables in the circuit, making the cycle-averaged model nonlinear, though still time invariant.

### B. Fourier Analysis

To derive an Index-0 cycle-averaged model, one needs to find nominal values at which to fix the Index-1 and higher cycle averages. From simulations of the SPCVM, we justified that the Index-2 and higher cycle averages can be neglected for all the SPCVM waveforms except the ventricular volume $Q_h$ and the ventricular elastance $E_h$. We then numerically (or partially analytically in the case of $s_1$ and $E_h$) calculated the relevant Index-1 and Index-2 cycle averages using steady-state Fourier series representations of all the hemodynamic waveforms and switching functions from our simulations. The steady-state SPCVM waveforms we used were obtained from simulations with the nominal SPCVM parameters [1]. The results are shown in Table II.

In addition, we implemented an Index-0 dependence for the Index-1 cycle averages of the ABP, $V_{a1}^R$ and $V_{a1}^I$, and for the Index-1 cycle averages of the ventricular volume, $Q_{h1}^R$ and $Q_{h1}^I$. The latter four Index-1 cycle averages were scaled by $T$ and $V_{a0}$, since (11) and (10), respectively, show that pulse

[3]Other approximations for $t_D$ do not make this assumption; however, the improvement in results does not justify the added complexity.

TABLE II
VALUES OF CYCLE AVERAGES IN STEADY STATE

| Variable | $\langle\bullet\rangle_0$ | $\langle\bullet\rangle_1^R$ | $\langle\bullet\rangle_1^I$ | $\langle\bullet\rangle_2^R$ | $\langle\bullet\rangle_2^I$ |
|---|---|---|---|---|---|
| $V_v$ | 15.23 | −0.09 | −0.03 | 0.02 | 0.01 |
| $V_a$ | 100.54 | −4.91 | −3.59 | −1.91 | 0.83 |
| $Q_h$ | 88.12 | 18.48 | 10.52 | 2.03 | −2.52 |
| $E_h$ | 0.70 | −0.09 | −0.47 | −0.21 | 0.12 |
| $s_1$ | 0.50 | 0.00 | 0.32 | 0 | 0 |
| $s_D$ | 0.25 | 0.06 | −0.22 | −0.14 | −0.08 |

pressure and stroke volume are proportional to $V_{a0}T$ in the Windkessel model. We therefore set

$$V_{a1}^R = \frac{V_{a0}}{V_{a0\text{nominal}}}\frac{T}{T_{\text{nominal}}}\left(V_{a1}^R\right)_{\text{nominal}} \tag{31}$$

$$V_{a1}^I = \frac{V_{a0}}{V_{a0\text{nominal}}}\frac{T}{T_{\text{nominal}}}\left(V_{a1}^I\right)_{\text{nominal}} \tag{32}$$

$$Q_{h1}^R = \frac{V_{a0}}{V_{a0\text{nominal}}}\frac{T}{T_{\text{nominal}}}\left(Q_{h1}^R\right)_{\text{nominal}} \tag{33}$$

$$Q_{h1}^I = \frac{V_{a0}}{V_{a0\text{nominal}}}\frac{T}{T_{\text{nominal}}}\left(Q_{h1}^I\right)_{\text{nominal}} \tag{34}$$

where the nominal values of the Index-1 cycle averages were taken from Table II. (One could also consider scaling the Index-2 cycle averages $Q_{h2}^I$ and $Q_{h2}^R$ by the same factor as in (31)–(34). However, from simulations of the Index-0 cycle-averaged model, we observed that such a scaling increases the resulting error, perhaps because the phase relations of the Index-1 and Index-2 terms change in the pulsatile circuit as conditions change.)

### C. Index-0 Cycle-Averaged Model

Using the values listed in Table II and applying the cycle-average operators from the previous section to (13)–(15), we obtain an Index-0 cycle-averaged model

$$\begin{aligned}\frac{d}{dt}\mathbf{X}_0(t) &= \frac{d}{dt}\begin{bmatrix} Q_{h0}(t) \\ V_{a0}(t) \\ V_{v0}(t)\end{bmatrix} \\ &= \begin{bmatrix} -\frac{\langle s_1 E_h Q_h\rangle_0}{R_1} - \frac{\langle s_D E_h Q_h\rangle_0}{R_2} + \frac{\langle s_D V_a\rangle_0}{R_2} + \frac{\langle s_1 V_v\rangle_0}{R_1} \\ \frac{\langle s_D E_h Q_h\rangle_0}{R_1 C_a} - \frac{(R_2+R_3)V_{a0}}{R_2 R_3 C_a} + \frac{V_{v0}}{R_3 C_a} \\ \frac{\langle s_1 E_h Q_h\rangle_0}{R_1 C_v} + \frac{V_{a0}}{R_3 C_v} - \frac{\langle s_1 V_v\rangle_0}{R_1 C_v} - \frac{V_{v0}}{R_3 C_v}\end{bmatrix}\end{aligned} \tag{35}$$

where the time argument $t$ has again been dropped for notational simplicity. Under our assumptions on the Index-1 and higher cycle averages, we can rewrite (35), using (20)–(25), as

$$\begin{aligned}\frac{d}{dt}\mathbf{X}_0(t) \approx\ & \mathcal{C}\left(S_{10}, S_{D0}(t), p\right)\mathbf{X}_0(t) \\ & + \mathbf{d}\left(S_{10}, S_{D0}(t), S_{11}, S_{D1}, \mathbf{X}_1, \mathbf{X}_2, p\right)\end{aligned} \tag{36}$$

where $\mathcal{C}(S_{10}, S_{D0}(t), p)$ is dependent on the Index-0 cycle averages of the switching functions and the parameters $p$, and where $\mathbf{d}(S_{10}, S_{D0}(t), S_{11}, S_{D1}, \mathbf{X}_1, \mathbf{X}_2, p)$ is dependent on the Index-0 and Index-1 cycle averages of the switching functions, the Index-1 cycle averages, $\mathbf{X}_1$, the Index-2 cycle averages of $Q_h$ and $E_h$, $\mathbf{X}_2$, and the parameters $p$. [Because of the Index-1 adjustments in (31)–(34), $\mathbf{X}_1$ actually varies with $\mathbf{X}_0(t)$.]

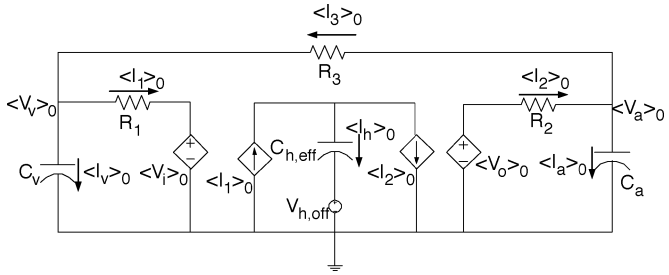


Fig. 6. Index-0 cycle-averaged model with two voltage-dependent voltage sources and two current-dependent current sources.

Note that the state variables in this cycle-averaged model are the Index-0 cycle averages of the state variables in the SPCVM. Furthermore, it can be verified that the total charge in this cycle-averaged model is conserved, and is equal to the total cycle-averaged charge in the SPCVM.

Initially, the parameters $p$ in $\mathcal{C}$ and $\mathbf{d}$ are set to the nominal SPCVM parameters in [1], which we shall call the nominal parameter set $p_{\text{nom}}$, and the Index-1 and Index-2 cycle averages are fixed at the values given in Table II. To start the cycle-averaged model in steady state, the initial conditions $\mathbf{X}_0(0)$ for the Index-0 cycle-averaged model are set equal to the numerically calculated cycle averages of the steady-state simulated waveforms, $\mathbf{x}_{ss}$, of the SPCVM using the parameters $p_{\text{nom}}$.

Due to truncation error in the Fourier series approximations leading to (36), however, setting $\mathbf{X}_0(0) = \mathbf{x}_{ss}$ in the Index-0 cycle-averaged model leads to a nonzero value for

$$\begin{aligned}\mathbf{e} = & \mathcal{C}\left(S_{10}, S_{D0}(0), p_{\text{nom}}\right)\mathbf{x}_{ss} \\ & + \mathbf{d}\left(S_{10}, S_{D0}(0), S_{11}, S_{D1}, \mathbf{X}_1, \mathbf{X}_2, p_{\text{nom}}\right)\end{aligned} \tag{37}$$

in the Index-0 cycle-averaged model. This violates the assumption that the circuit starts in steady state with a fixed charge (or blood volume). To correct for this truncation error, we can subtract the fixed correction term $\mathbf{e}$ from the right side of (36). The Index-0 cycle-averaged model we propose is then given by

$$\begin{aligned}\frac{d}{dt}\mathbf{X}_0(t) = & \mathcal{C}\left(S_{10}, S_{D0}(t), p\right)\mathbf{X}_0(t) \\ & + \mathbf{d}\left(S_{10}, S_{D0}(t), S_{11}, S_{D1}, \mathbf{X}_1, \mathbf{X}_2, p\right) - \mathbf{e}.\end{aligned} \tag{38}$$

One alternative to using this correction term would be to use more Index-2 Fourier series terms in (36); such higher-order approximations were only used for expressions involving $Q_h$ and $E_h$.

We can also construct a circuit model that captures the dynamics of the Index-0 cycle-averaged model using voltage-dependent voltage sources and current-dependent current sources. Such an Index-0 cycle-averaged circuit, based on the SPCVM state space model in (13) through (15) (or by direct averaging of the circuit in Fig. 2, see [18]), is shown in Fig. 6. Note that the LTI components of the pulsatile circuit are unchanged by the cycle averaging; they are in the same location, imposing the same constraints, but now on the averaged rather than instantaneous quantities. In this averaged circuit, the average compliance for the left ventricle, $C_{h,\text{eff}}$, is equal to $1/E_{h0}$ (see [13]

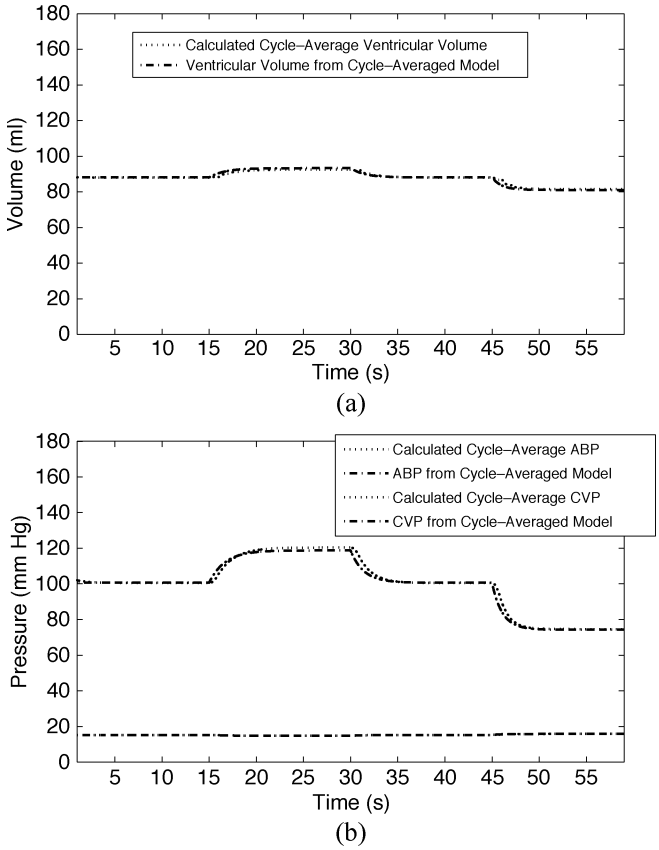


Fig. 7. Comparison of the transient responses of the Index-0 cycle-averaged model to the calculated cycle-averaged SPCVM waveforms for several step changes in resistance $R_3$. At $t = 15$ s, $R_3$ was stepped up to 1.4 PRU, at $t = 30$ s, $R_3$ was stepped down to 1 PRU, and at $t = 45$ s, $R_3$ was stepped down to 0.6 PRU. (a) Ventricular volume. (b) ABP and central venous pressure.

for a derivation), and the source $V_{h,\text{eff}}$ is introduced to properly convert $Q_{h0}$ into $V_{h0}$. Using $V_i$ and $V_o$ from the circuit in Fig. 2, we can write

$$V_{i0} = S_{10}V_{h0} + (1 - S_{10})\,V_{v0} + K_i \tag{39}$$

$$V_{o0} = S_{D0}V_{h0} + (1 - S_{D0})\,V_{a0} + K_o \tag{40}$$

where $K_i$ and $K_o$ are introduced from the Index-1 cycle averages of $s_D$, $V_h$, $V_a$, and $V_v$, and fixed Index-2 cycle averages of $E_h$ and $Q_h$.

## VI. Results and Discussion

Using the Index-0 cycle-averaged model (38), we obtained simulation results for typical transient responses to step changes in $R_3$, the systemic vascular resistance, and in $T$, the length of the cardiac cycle. We decided on these two parameters because both are significant hemodynamic variables in the clinical setting, and the cycle-averaged model is sensitive to both.

Fig. 7 shows the transient responses of the Index-0 cycle-averaged model for $T = 1$ s, during three step changes in systemic vascular resistance $R_3$ [in peripheral resistance units (PRU) or equivalently mmHg/(ml/s)]: at $t = 15$ s, $R_3$ was stepped up to 1.4 PRU; at $t = 30$ s, $R_3$ was stepped down to 1 PRU; and at $t = 45$ s, $R_3$ was stepped down to 0.6 PRU. In Fig. 7, the Index-0 cycle-averaged model responses are compared to the calculated Index-0 cycle averages from the SPCVM.

TABLE III
Steady-State Error for the Values of $R_3$ From Fig. 7

| | Steady-state Error (%) for specified values of $R_3$ in: | | |
|---|---|---|---|
| $R_3$ in PRU | $V_a$ | $Q_h$ | $V_v$ |
| 1 | 0.00 | 0.00 | 0.00 |
| 0.6 | 0.54 | 0.55 | 0.04 |
| 1.4 | 1.33 | 0.86 | 0.14 |

TABLE IV
Time Constants in Steady State for the Transient Responses for the Values of $R_3$ From Fig. 7

| $R_3$ in PRU | Analytical Time Constant | Calculated Time Constant | $R_3C_a$ |
|---|---|---|---|
| 1.4 | 1.21 s | 1.17 s | 2.8 s |
| 1 | 1.05 s | 1.06 s | 2 s |
| 0.6 | 0.82 s | 0.98 s | 1.2 s |

The errors inherent in the steady-state cycle-averaged waveforms for ABP, ventricular volume, and CVP from this simulation are shown in Table III. The maximum error in the steady-state cycle-averaged waveforms (i.e., after each transient step response has settled) was approximately 1.3%, which is acceptable for the applications envisioned for this model. For this simulation, the transient error is lower than the steady-state error and is not reported here. There was no error for the nominal condition of $R_3 = 1$ PRU because the initial conditions of the model (38) were set such that we began the simulation at the calculated cycle averages from a simulation of the SPCVM with $p = p_{\text{nom}}$, and $\mathbf{X}_1$ and $\mathbf{X}_2$ set to the values given in Table II.

In steady state, the matrix $\mathcal{C}(S_{10}, S_{D0}(t), p)$ has three eigenvalues: one corresponding to a fast time constant (≈0.02 s), another to a slow time constant, and one that is zero [13]. The transient responses on the time scales of our simulation are governed by the slow time constant. For the simulation of transients in $R_3$ in Fig. 7, we determined the slow time constant both analytically and empirically in the neighborhood of steady state. We computed analytical time constants by calculating the eigenvalues of $\mathcal{C}(S_{10}, S_{D0}(t), p)$ at $t = 30$ s ($R_3 = 1.4$ PRU), $t = 45$ s ($R_3 = 1$ PRU), and $t = 60$ s ($R_3 = 0.6$ PRU). We also computed empirical time constants by fitting an exponential function to the calculated cycle-averaged ABP waveform for $24 < t < 30$ s ($R_3 = 1.4$ PRU), $39 < t < 45$ s ($R_3 = 1$ PRU), and $54 < t < 60$ s ($R_3 = 0.6$ PRU). Table IV compares these two time constants to that obtained by estimating the time constant as $R_3C_a$, a reasonable assumption for the SPCVM since $C_v$ is large and the SPCVM spends most of the cardiac cycle with $s_D(t) = 0$. The empirical time constant for $R_3 = 0.6$ PRU does not match the analytical one as well as the other cases because the transient response for $45 < t < 60$ s settles to steady state very quickly, making it difficult to properly estimate the time constant. Nonetheless, the analytical time constants we obtained are much more accurate than simply estimating the time constant as $R_3C_a$.

Fig. 8 shows the transient responses of the Index-0 cycle-averaged model for three step changes in cardiac cycle duration $T$: at $t = 15$ s, $T$ was stepped down to 0.5 s; at $t = 30$ s, $T$ was stepped back up to its nominal value of 1 s; and at $t = 45$ s, $T$ was stepped up to 1.2 s. These values of $T$ correspond to heart rates of 50 beats per minute (bpm)

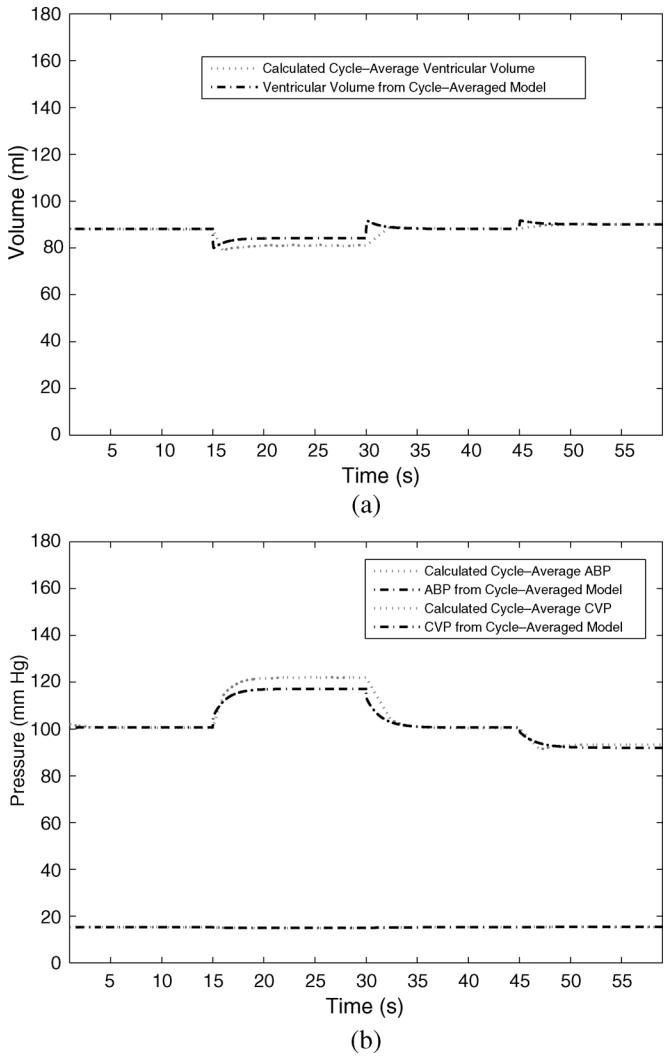


Fig. 8. Comparison of the transient responses of the Index-0 cycle-averaged model to the calculated cycle-averaged SPCVM waveforms for several step changes in $T$. At $t = 15$ s, $T$ was stepped down to 0.5 s. At $t = 30$ s, $T$ was stepped back up to its nominal value of 1 s, and at $t = 45$ s, $T$ was stepped up to 1.2 s. (a) Ventricular volume. (b) ABP and central venous pressure.

to 120 bpm. In Fig. 8, the Index-0 cycle-averaged model responses are compared to the calculated Index-0 cycle averages from the SPCVM. The maximum error in the steady-state cycle-averaged waveforms is larger than the simulation with transient changes in $R_3$—approximately 4%. This happens when the heart rate goes high, and where our approximation for $t_D$ is poorest. For heart rate going low, the maximum error is 1.5%. Again, for this simulation, the transient error is lower than the steady-state error.

There are significant computational savings obtained when using the Index-0 cycle-averaged model. Table V compares the CPU time for the simulation of Fig. 7 versus the time that it would take to simulate the SPCVM for the transients in $R_3$, not including the computational time for the calculated averages in Fig. 7. For the simulations, we used a Pentium M 1.7 GHz personal computer running Windows XP and MATLAB 7.01 (The Mathworks Inc., Natick, MA) with the "ode23" differential

TABLE V
COMPUTATIONAL SAVINGS OBTAINED USING THE INDEX-0 CYCLE-AVERAGED MODEL

| Model | CPU Time | Max. Step Size Limit |
|---|---|---|
| SPCVM | 6.05 s | 0.004 s |
| Index-0 CAM | 0.61 s | 0.5 s |

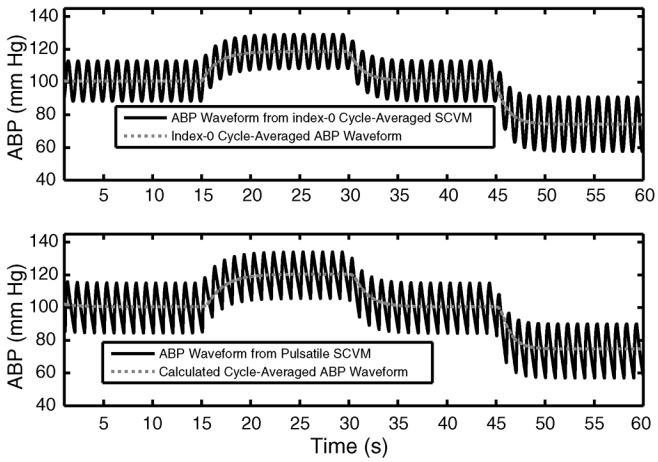


Fig. 9. Envelope of the ABP waveform from the cycle-averaged model (top) compared to that of the SPCVM (bottom) for several step changes in peripheral resistance $R_3$. At $t = 15$ s, $R_3$ was stepped up to 1.4 PRU, at $t = 30$ s, $R_3$ was stepped down to 1 PRU, and at $t = 45$ s, $R_3$ was stepped down to 0.6 PRU.

equation solver. In the table, we also list the maximum step size limits that can be used in the simulations before output waveform degradation occurs.

Finally, we note that systolic and diastolic ABP, both important variables in clinical settings, can be estimated from the Index-0 cycle-averaged model. Fig. 9 is an example of such an approximation, where the ABP waveforms from the cycle-averaged model and the SPCVM are compared for the same transient as that in Fig. 7. The waveform in the top of Fig. 9 is sinusoidal, as it was calculated using the formula

$$V_a(t) \approx V_{a0}(t) + 2V_{a1}^R \cos\left(\frac{2\pi}{T}t\right) - 2V_{a1}^I \sin\left(\frac{2\pi}{T}t\right) \quad (41)$$

with $V_{a1}^R$ and $V_{a1}^I$ modulated as in (31) and (32), respectively.

## VII. CONCLUSION

We have presented a cycle-averaging methodology applicable to dynamic systems in close to periodic operation, and illustrated it by application to the classical Windkessel model of cardiovascular dynamics and to a somewhat more elaborate cardiovascular model—the SPCVM—that has nonlinear and time-varying components. The cycle-averaged models are derived by applying short-term averaging operators to the differential equations of the underlying pulsatile models, rather than by introducing heuristic averaging during the model-building step, as is done in existing nonpulsatile models. Despite the approximations needed to obtain the cycle-averaged version of SPCVM, our averaged model captures the intercycle cardiovascular dynamics of SPCVM with relatively small approximation errors

for a large range of perturbations in important system parameters. Further simplifications of the SPCVM—for instance, replacing $V_v$ by a constant source, eliminating the diode, and simplifying the logic for the switch—lead to pulsatile behavior that is still representative of cardiovascular dynamics, but that may have a simpler averaged model. In ongoing work, we are exploring such simplifications, various extensions, and applications to fitting real data collected in the ICU by estimating model states and parameters. In particular, we are exploring the use of cycle-averaged models that capture beat-to-beat variability in ABP waveforms to estimate important hemodynamic variables such as stroke volume, ejection fraction, arterial resistance, and cardiac output.

## APPENDIX I
## EXPRESSIONS USED IN THE INDEX-0 MODEL

In this appendix, we give the expressions used for $\mathcal{C}(S_{10}, S_{D0}(t), p)$ and $\mathbf{d}(S_{10}, S_{D0}(t), S_{11}, S_{D1}, \mathbf{X}_1, \mathbf{X}_2, p)$. These expressions were derived using the approximations in (20)–(25).

The entries of the $3 \times 3$ matrix

$$\mathcal{C}\left(S_{10}, S_{D0}(t), p\right) = \begin{bmatrix} c_{11} & c_{12} & c_{13} \\ c_{21} & c_{22} & c_{23} \\ c_{31} & c_{32} & c_{33} \end{bmatrix}$$

are as follows:

$$\begin{aligned} c_{11} = &-\frac{S_{10}E_{h0}}{R_1} - \frac{S_{D0}E_{h0}}{R_2} - 2\frac{{S_{D1}}^R {E_{h1}}^R}{R_2} \\ &- 2\frac{{S_{D1}}^I {E_{h1}}^I}{R_2} - 2\frac{{S_{11}}^R {E_{h1}}^R}{R_1} - 2\frac{{S_{11}}^I {E_{h1}}^I}{R_1} \end{aligned} \tag{42}$$

$$c_{12} = \frac{S_{D0}}{R_2} \tag{43}$$

$$c_{13} = \frac{S_{10}}{R_1} \tag{44}$$

$$c_{21} = \frac{S_{D0}E_{h0}}{C_a R_2} + 2\frac{{S_{D1}}^R {E_{h1}}^R}{C_a R_2} + 2\frac{{S_{D1}}^I {E_{h1}}^I}{C_a R_2} \tag{45}$$

$$c_{22} = -\frac{R_2 + R_3 S_{D0}}{C_a R_2 R_3} \tag{46}$$

$$c_{23} = \frac{1}{C_a R_3} \tag{47}$$

$$c_{31} = \frac{S_{10}E_{h0}}{C_v R_1} + 2\frac{{S_{11}}^R {E_{h1}}^R}{C_v R_1} + 2\frac{{S_{11}}^I {E_{h1}}^I}{C_v R_1} \tag{48}$$

$$c_{32} = \frac{1}{C_v R_3} \tag{49}$$

$$c_{33} = -\frac{R_3 S_{10} + R_1}{C_v R_1 R_3}. \tag{50}$$

The entries of the $3 \times 1$ vector

$$\mathbf{d}\left(S_{10}, S_{D0}(t), S_{11}, S_{D1}, \mathbf{X}_1, \mathbf{X}_2, p\right) = \begin{bmatrix} d_1 \\ d_2 \\ d_3 \end{bmatrix}$$

are given below. The expressions simplify somewhat under the reasonable assumption that ${V_{v1}}^R$ and ${V_{v1}}^I$ are negligibly small

$$\begin{aligned} d_1 = &-2\left({Q_{h1}}^R {E_{h1}}^R + {Q_{h1}}^I {E_{h1}}^I\right)\left(\frac{S_{10}}{R_1} + \frac{S_{D0}}{R_2}\right) \\ &- 2\left({Q_{h2}}^R {E_{h2}}^R + {Q_{h2}}^I {E_{h2}}^I\right)\left(\frac{S_{10}}{R_1} + \frac{S_{D0}}{R_2}\right) \\ &- 2\left(\frac{{S_{D1}}^R E_{h0} {Q_{h1}}^R + {S_{D1}}^I E_{h0} {Q_{h1}}^I}{R_2}\right) \\ &- 2\left(\frac{{S_{11}}^R E_{h0} {Q_{h1}}^R + {S_{11}}^I E_{h0} {Q_{h1}}^I}{R_1}\right) \\ &- 2\left(\frac{{S_{D1}}^R {V_{a1}}^R + {S_{D1}}^I {V_{a1}}^I}{R_2}\right) \\ &+ 2\left(\frac{{S_{11}}^R {V_{v1}}^R + {S_{11}}^I {V_{v1}}^I}{R_1}\right) \\ &- 2\left(\frac{{S_{11}}^R}{R_1} + \frac{{S_{D1}}^R}{R_2}\right)\left({Q_{h2}}^R {E_{h1}}^R + {Q_{h2}}^I {E_{h1}}^I\right) \\ &- 2\left(\frac{{S_{11}}^R}{R_1} + \frac{{S_{D1}}^R}{R_2}\right)\left({Q_{h1}}^R {E_{h2}}^R + {Q_{h1}}^I {E_{h2}}^I\right) \\ &- 2\left(\frac{{S_{11}}^I}{R_1} + \frac{{S_{D1}}^I}{R_2}\right)\left({Q_{h2}}^R {E_{h1}}^I - {Q_{h2}}^I {E_{h1}}^R\right) \\ &- 2\left(\frac{{S_{11}}^I}{R_1} + \frac{{S_{D1}}^I}{R_2}\right)\left({Q_{h1}}^R {E_{h2}}^I - {Q_{h1}}^I {E_{h2}}^R\right) \end{aligned} \tag{51}$$

$$\begin{aligned} d_2 = &2S_{D0}\left(\frac{{Q_{h1}}^R {E_{h1}}^R + {Q_{h1}}^I {E_{h1}}^I}{C_a R_2}\right) \\ &+ 2S_{D0}\left(\frac{{Q_{h2}}^R {E_{h2}}^R + {Q_{h2}}^I {E_{h2}}^I}{C_a R_2}\right) \\ &+ 2\left(\frac{{S_{D1}}^R E_{h0} {Q_{h1}}^R + {S_{D1}}^I E_{h0} {Q_{h1}}^I}{C_a R_2}\right) \\ &- 2\left(\frac{{S_{D1}}^R {V_{a1}}^R + {S_{D1}}^I {V_{a1}}^I}{C_a R_2}\right) \\ &+ 2\frac{{S_{D1}}^R}{C_a R_2}\left({Q_{h2}}^R {E_{h1}}^R + {Q_{h2}}^I {E_{h1}}^I\right) \\ &+ 2\frac{{S_{D1}}^R}{C_a R_2}\left({Q_{h1}}^R {E_{h2}}^R + {Q_{h1}}^I {E_{h2}}^I\right) \\ &+ 2\frac{{S_{D1}}^I}{C_a R_2}\left({Q_{h2}}^R {E_{h1}}^I - {Q_{h2}}^I {E_{h1}}^R\right) \\ &+ 2\frac{{S_{D1}}^I}{C_a R_{2q}}\left({Q_{h1}}^R {E_{h2}}^I - {Q_{h1}}^I {E_{h2}}^R\right) \end{aligned} \tag{52}$$

$$\begin{aligned} d_3 = &2S_{10}\left(\frac{{Q_{h1}}^R {E_{h1}}^R + {Q_{h1}}^I {E_{h1}}^I}{C_v R_1}\right) \\ &+ 2S_{10}\left(\frac{{Q_{h2}}^R {E_{h2}}^R + {Q_{h2}}^I {E_{h2}}^I}{C_v R_1}\right) \\ &+ 2\left(\frac{{S_{11}}^R E_{h0} {Q_{h1}}^R + {S_{11}}^I E_{h0} {Q_{h1}}^I}{C_v R_1}\right) \end{aligned}$$

$$
\begin{aligned}
&- 2\left(\frac{S_{11}^{R}V_{v1}^{R} + S_{11}^{I}V_{v1}^{I}}{C_v R_1}\right) \\
&+ 2\frac{S_{11}^{R}}{C_v R_1}\left(Q_{h2}^{R}E_{h1}^{R} + Q_{h2}^{I}E_{h1}^{I}\right) \\
&+ 2\frac{S_{11}^{R}}{C_v R_1}\left(Q_{h1}^{R}E_{h2}^{R} + Q_{h1}^{I}E_{h2}^{I}\right) \\
&+ 2\frac{S_{11}^{I}}{C_v R_1}\left(Q_{h2}^{R}E_{h1}^{I} - Q_{h2}^{I}E_{h1}^{R}\right) \\
&+ 2\frac{S_{11}^{I}}{C_v R_1}\left(Q_{h1}^{R}E_{h2}^{I} - Q_{h1}^{I}E_{h2}^{R}\right). \qquad (53)
\end{aligned}
$$

## REFERENCES


[1] T. A. Parlikar and G. C. Verghese, "A simple cycle-averaged model of cardiovascular dynamics," in *Proc. 27th Ann. Conf. IEEE Engineering in Medicine and Biology Society 2005*, Sep. 2005, pp. 5490–5494.

[2] O. Frank, "Die Grundform des arteriellen Pulses. Erste Abhandlung. Mathematische Analyse," *Z. f. Biol.*, vol. 37, pp. 485–526, 1899.

[3] K. Sagawa, R. K. Lie, and J. Schaefer, "Translation of Otto Frank's paper "Die Grundform des arteriellen Pulses"," *J. Mol. Cell. Cardiol.*, vol. 22, pp. 253–277, 1990.

[4] O. Frank, "Schäatzung des Schlagvolumens des menschlichen Herzens auf Grund der Wellen- und Windkesseltheorie," *Z. f. Biol.*, vol. 90, pp. 405–409, 1930.

[5] A. Noordergraaf, "Development of an analog computer for the human systemic circulatory system," in *Circulatory Analog Computers*, A. Noordergraaf, G. Jager, and N. Westerhof, Eds. Amsterdam, Holland: North-Holland, 1963, pp. 29–44.

[6] T. L. Davis and R. G. Mark, "Teaching physiology through interactive simulation of hemodynamics," *Comput. Cardiol.*, pp. 649–652, Sep. 1990.

[7] R. Beeukes and N. Braslow, "The cardiovascular analog trainer: A real time physiological simulator," *Physiol. Teacher*, vol. 3, no. 3, pp. 4–7, 1974.

[8] M. Saeed, C. Lieu, G. Raber, and R. Mark, "MIMIC II: A massive temporal ICU patient database to support research in intelligent patient monitoring," *Comput. Cardiol.*, vol. 29, pp. 641–644, 2002.

[9] F. S. Grodins, "Integrative cardiovascular physiology: A mathematical synthesis of cardiac and blood vessel hemodynamics," *Q. Rev. Biol.*, vol. 34, pp. 93–116, Jun. 1959.

[10] F. Kappel and R. O. Peer, "Fundamental regulation processes in the cardiovascular system," *J. Math. Biol.*, vol. 31, pp. 611–631, 1993.

[11] D. Boyers, J. Cuthbertson, and J. Luetscher, "Simulation of the human cardiovascular system: A model with normal response to change in posture, blood loss, transfusion, and autonomic blockade," *Simulation*, vol. 18, pp. 197–205, 1972.

[12] G. C. Verghese, "Dynamic modeling and control in power electronics," in *The Control Handbook*, W. S. Levine, Ed. Boca Raton, FL: CRC, 1996, pp. 1413–1424.

[13] T. Heldt, J. Chang, J. Chen, G. Verghese, and R. Mark, "Cycle-averaged dynamics of a periodically-driven, closed-loop circulation model," *Cont. Eng. Practice*, vol. 13, pp. 1163–1171, 2005.

[14] H. Raymundo, A. M. Scher, D. S. O'Leary, and P. D. Sampson, "Cardiovascular control by arterial and cardiopulmonary baroreceptors in awake dogs with atrioventricular block," *Amer. J. Physiol.*, vol. 257, no. 26, pp. H2048–H2058, 1989.

[15] J. E. A. James and M. D. B. Daly, "Comparison of the reflex vasomotor responses to separate and combined stimulation of the carotid sinus and aortic arch baroreceptors by pulsatile and nonpulsatile pressures in the dog," *J. Physiol.*, vol. 209, no. 2, pp. 257–293, 1970.

[16] S. R. Sanders, J. M. Noworolski, X. Z. Liu, and G. C. Verghese, "Generalized averaging method for power conversion circuits," *IEEE Trans. Power Electron.*, vol. 6, no. 4, pp. 251–259, Apr. 1991.

[17] V. A. Caliskan, G. C. Verghese, and A. M. Stankovic, "Multi-frequency averaging of dc/dc converters," *IEEE Trans. Power Electron.*, vol. 14, no. 1, pp. 124–133, Jan. 1999.

[18] J. G. Kassakian, M. F. Schlecht, and G. C. Verghese, *Principles of Power Electronics*. Reading, MA: Addison-Wesley, 1991.

[19] J. J. S. Chen, T. Heldt, G. C. Verghese, and R. G. Mark, "Analytical solution to simplified circulatory model using piecewise-linear elastance function," *Comput. Cardiol.*, vol. 30, pp. 259–262, 2003.

[20] G. Rosenberg, W. M. Phillips, D. L. Landis, and W. S. Pierce, "Design and evaluation of the Pennsylvania State University mock circulation system," *Amer. Soc. Artif. Internal Organs (ASAIO) J.*, vol. 4, pp. 41–49, 1981.

[21] H. Senzaki, C. H. Chen, and D. A. Kass, "Single-beat estimation of end-systolic pressure-volume relation in humans," *Circulation*, vol. 94, pp. 2497–2506, 1994.

[22] T. Heldt, "Modeling of the cardiovascular response to orthostatic stress," Ph.D. thesis, Division of Health Sciences and Technology, M.I.T , Cambridge, Sep. 2004.


**Tushar A. Parlikar** (S'98) received the B.S. degree in engineering and the B.A. degree in mathematics from Swarthmore College, Swarthmore, PA, in 2001, and the Master's degree from the Massachusetts Institute of Technology (MIT), Cambridge, in 2003. He is currently a working toward the Ph.D. degree at the Laboratory for Electromagnetic and Electronic Systems, MIT, investigating the use of physiological models and model-based estimation methods for patient monitoring.

His research interests include dynamic systems modeling, estimation, and control, and applications in fields such as power electronics, automotive systems, and biological systems.

Mr. Parlikar was awarded the Thomas McCabe award given to the most outstanding engineering student in the senior class, when he was an undergraduate at Swarthmore College. He is a member of Sigma Xi, Tau Beta Pi, and Phi Beta Kappa.

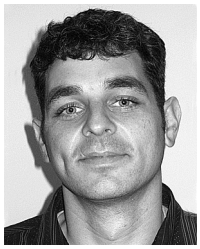

**Thomas Heldt** (M'06) studied physics at the Johannes Gutenberg-Universität, Mainz, Germany, and received the M.S. and M.Phil. degrees in physics from Yale University, New Haven, CT, and the Ph.D. degree in medical physics from the Harvard University-Massachusetts Institute of Technology (MIT) Division of Health Sciences and Technology, MIT, Cambridge.

He is currently a Post-Doctoral Researcher with the Laboratory for Electromagnetic and Electronic Systems, MIT. His research interests include mathematical modeling of physiological systems, model reduction, and model identification, particularly as they pertain to patient monitoring and spaceflight applications.

**George C. Verghese** (S'74–M'78–SM'97– F'98) received the B.Tech. degree from the Indian Institute of Technology, Madras, India, the M.S. degree from the State University of New York, Stony Brook, and the Ph.D. degree from Stanford University, Stanford, CA, all in electrical engineering.

He joined the Electrical Engineering and Computer Science Department, MIT, in 1979, where he is a Professor of Electrical Engineering, attached to the Laboratory for Electromagnetic and Electronic Systems. His research interests are in modeling the structure and dynamics of complex networks and systems, model reduction, identification, and control, particularly for biomedical and electric power applications. He is coauthor of *Principles of Power Electronics* (Addison-Wesley, 1991).

Dr. Verghese has served terms as Associate Editor of *Automatica* and of the IEEE TRANSACTIONS ON AUTOMATIC CONTROL and IEEE TRANSACTIONS ON CONTROL SYSTEMS TECHNOLOGY. He has also served on the AdCom of the IEEE Power Electronics Society.